ChemElectroChem

Research Article
doi.org/10.1002/celc.202200800

Chemistry Europe
European Chemical Societies Publishing

www.chemelectrochem.org

Pseudohexagonal Nb_2O_5-Decorated Carbon Nanotubes as a High-Performance Composite Anode for Sodium Ion Batteries

Guanxu Chen,[a] Jintao Chen,[b] Ivan P. Parkin,[b] Guanjie He,*[a, b, c] and Thomas S. Miller*[a]

To promote the commercial application of sodium ion batteries (SIBs), new high-stability and high-capacity anode materials are needed. Metal oxides show great promise, but significant issues relating to their low electrical conductivity and unstable structure during charge storage must be resolved. Herein, a new composite anode consisting of pseudohexagonal Nb_2O_5 (TT-Nb_2O_5) nanoparticles strongly anchored to carbon nanotubes (CNT) through a glucose-derived carbon framework (Nb_2O_5/g-CNT) was synthesised and assessed for use as the anode in SIBs. This represents the first application of TT-Nb_2O_5 in SIBs. The composite is shown to offer high specific capacity (203 mAh g^{-1} at 0.2 A g^{-1}), good rate capability (53 mAh g^{-1} at high current density of 5 A g^{-1}), and a high-capacity retention rate (135 mAh g^{-1} at 0.2 A g^{-1} between 25 and 300 cycles). This is attributed to high electrical conductivity and flexibility offered by the designed carbon framework, the superior capacity of the TT-Nb_2O_5 and the linkage between the two provided by the bonding glucose derived carbon. This work therefore demonstrates a scalable route for the application of metal oxides in future high-performance SIB systems.

Introduction

Sodium ion batteries (SIBs) are promising alternatives to current lithium-ion batteries (LIBs) in large-scale energy storage systems because of the high abundance, low cost and equitable distribution of Na globally.[1] However, the practical application of SIBs is still challenging due to their relatively poor cycling stability and lower energy density when compared to LIBs.[2,3] This is in part due to the need to use hard carbon as their active anode material, as opposed to graphite which is used in LIBs, which offers limited capacity and slow kinetics (~341 mAh g^{-1} at a very slow rate of 0.02 A g^{-1}).[4–6] New carbonaceous (e.g. carbon nano-fibres (CNFs), graphene[7–11]) and non-carbonaceous (e.g. $Na_2Ti_3O_7$, Co_3O_4–Fe_2O_3[12–16]) SIB anode materials have been investigated, but both systems have been found to have problems.[2,17,18] While transition metal oxides have high theoretical capacities for Na and wide potential windows, and hence offer significant energy densities,[19] they commonly suffer from poor electrical conductivity and low first-cycle Coulombic efficiency (FCCE). Conversely novel carbon materials have high electrical conductivities and reasonable specific capacities, but also suffer from low Coulombic efficiency.[20] For example multi-walled carbon nanotubes (MWCNTs) have good structural flexibility and a very high conductivity of ~49 S cm^{-1},[21] but they alone are unfavourable as an anode for SIBs due to their limited Na storage capacity (~28 mAh g^{-1} at 0.025 A g^{-1} after 50 cycles)[22] and relatively poor stability.[23,24] However, by compositing metal oxides and novel carbon frameworks, many of the limitations of the individual materials can be overcome.[25–27]

Niobium pentoxide (Nb_2O_5) can store Li ions through an intercalation mechanism and it has been explored as a potential anode material for high-rate Li-ion storage systems with a theoretical capacity of ~404 mAh g^{-1}.[28–30] In LIBs, Nb_2O_5 has been shown to offer high-rate performance (43 mAh g^{-1} at 10 A g^{-1})[31] and its high potential window can help to prevent the formation of lithium dendrites during cycling.[11] Both the crystalline orthorhombic (T-) and pseudohexagonal (TT-) Nb_2O_5 are considered to be promising materials for SIBs due to their kinetically fast intercalation/de-intercalation abilities. Unfortunately, T-Nb_2O_5-based SIB anodes to date have shown unstable long cycle performance.[32–35] However the TT-Nb_2O_5 form of this material has not yet been studied in SIBs. Importantly, TT-Nb_2O_5 can formed at a lower calcination temperature (500 °C) than T-Nb_2O_5 (800 °C) meaning TT-Nb_2O_5 can have a smaller average particle size, which positively impacts battery capacity.[36] Moreover, the simpler synthesis of the TT form Nb_2O_5 should help to cut production costs and make niobium-based batteries more industrially scalable. To date two main approaches have been

[a] G. Chen, Dr. G. He, Dr. T. S. Miller
Electrochemical Innovation Lab
Department of Chemical Engineering, UCL
London, WC1E 7JE, UK
E-mail: g.he@ucl.ac.uk
t.miller@ucl.ac.uk
Homepage: https://iris.ucl.ac.uk/iris/browse/profile?upi=GJHEX85
https://iris.ucl.ac.uk/iris/browse/profile?upi=TSMIL33
[b] J. Chen, Prof. I. P. Parkin, Dr. G. He
Department of Chemistry
University College London
20 Gordon Street, London, WC1H 0AJ, UK
[c] Dr. G. He
School of Engineering and Materials Science
Queen Mary University of London
Mile End Road, London, E1 4NS, UK

Supporting information for this article is available on the WWW under https://doi.org/10.1002/celc.202200800

used to solve the problem of improving the electrical conductivity of Nb_2O_5: 1) by combining it with carbon-based conductive materials (e.g. graphene,[37–39] CNF,[35,40] carbon nanotubes (CNTs)[41,42]) or 2) reducing the size of the Nb_2O_5 particles to the nano-scale.[27,41,43–47]

In this study, a high-performance SIB anode material consisting of pseudohexagonal Nb_2O_5 (TT-Nb_2O_5) nanoparticles that are tightly anchored onto MWCNTs, via the use of a glucose derived bonding carbon layer (Nb_2O_5/g-CNT), is prepared; this is the first investigation of TT-Nb_2O_5 for SIBs. The resultant material is demonstrated to offer three significant advantages for use as a SIB anode: 1) the glucose-derived carbon acts to strongly bond the homogeneously wrapped Nb_2O_5 nanoparticles onto the MWCNTs, leading to significantly enhanced electrical conductivity and connectivity to the metal oxide, ensuring high material utilisation and fast kinetics; 2) the highly accessible surface area of the nanostructured composite improves the mass transport and rate performance; 3) The mechanical strength and flexibility of the CNT network support allows the electrode to endure mechanical stresses during cycling, e.g. via volume expansion, promoting long cell lifetimes. This work therefore offers a route to high-performance and low cost Nb_2O_5 based batteries.

Experimental Section

Synthesis of Nb_2O_5/g-CNT Composite

The Nb_2O_5/g-CNT composite was synthesised by a one-step hydrothermal method followed by annealing. First, 0.4 g ammonium niobate (V) oxalate hydrate (Sigma-Aldrich, UK), 35 mg multi-walled carbon nanotubes (MWCNTs, Sigma-Aldrich, UK) and 0.4 g glucose (Sigma-Aldrich, UK) were mixed and ground before they were added into 30 ml of methanol/deionised (DI) water (1:1 in volume ratio) solution under continuous stirring. The mixture was then sonicated in an ultrasonic bath for 3 hours to enable dissolution and homogenisation, before it was transferred into a Teflon-lined autoclave (Parr, US) and heated to 180 °C with a ramp rate of 20 °C/min, where it was held for 12 hours. After synthesis the resultant powder was centrifuged, washed with DI water three times and freeze-dried, before it was annealed in a tube furnace at 500 °C for 3 hours in an alumina crucible under argon flow. The pristine Nb_2O_5 was synthesised using the same method without the addition of glucose and MWCNTs, whereas for g-CNT the mix excluded the niobium precursor. The Nb_2O_5/g-CNT composite with lower carbon content was also synthesised by halving the amount of the carbon material precursors. For the mechanically mixed Nb_2O_5 + g-CNT material, the two components were homogeneously mixed together by grinding using a pestle mortar.

Material Characterisation

The crystal structure and phase of the products were confirmed by X-ray diffraction (XRD, STOE SEIFERT) with a Cu Kα radiation at a 2θ range of 10–80°. The morphology of the Nb_2O_5/g-CNT composite was observed by scanning electron microscopy (SEM, JEOL, JSM 6701 FEG-SEM), and transmission electron microscopy (TEM, JEOL, JEM-2100F) with an accelerating voltage of 200 kV. The surface chemistry of the Nb_2O_5/g-CNT composite was analysed by X-ray photoelectron spectroscopy (XPS, Thermo-Scientific, K-alpha photoelectron spectrometer). The XPS data was processed using Casa XPS with the C1s at 284.8 eV as the standard reference for calibration. The composition of the samples was analysed and calculated by the thermalgravimetric analysis (TGA, METTLER TOLEDO, TGA/DSC 3+). The BET surface area of the Nb_2O_5/g-CNT composite was measured by N_2 adsorption/desorption with activation temperature of 150 °C (BET, Micromeritics, Flex&3Flex).

Electrochemical Characterisation

The anodes were prepared by coating slurries of 70% active material, 10% super C65 conductive carbon black and 20% polyvinylidene fluoride (PVDF) in N-methyl-2-pyrrolidone (NMP), mixed using a Thinky Mixer (Thinky, ARE-250), onto an aluminium foil at ~25 μm, before they were dried at 120 °C for 12 hours in a vacuum oven. The electrochemical performance of the anodes was tested in CR2032 coin cells with a sodium metal foil (99.9% Sigma Aldrich) as the counter electrode, a glass fibre filter as the separator (Whatman, GF/D) and an electrolyte consisting of 1 M $NaPF_6$ in ethylene carbonate (EC)/diethyl carbonate (DEC) in a 1:1 volume ratio (fluorochem, UK). Cyclic voltammetry (CV) tests were performed using a potentiostat (Bio-logic, VSP-300) within the range of 0.01 to 3 V (vs. Na/Na^+) at scan rates from 0.1 mV s^{-1} to 0.5 mV s^{-1}, while the charge-discharge measurements were carried out using a battery tester (Neware, BTS4000) within the range of 0.01 to 3 V (vs. Na/Na^+). The pristine Nb_2O_5 and Nb_2O_5 + g-CNT electrodes were prepared by using the same method.

Results and Discussion

Hydrothermal synthesis is one of the most efficient methods for the production of nanomaterials[48] as the morphology of the hydrothermal product can easily be controlled by changing the reaction conditions (e.g. temperature, time and precursors). Hence, here the Nb_2O_5/g-CNT composite was synthesised using a one-step hydrothermal method followed by an annealing step (Figure SI.1) to optimise the crystallinity of as-synthesised samples. It has been reported in literature that different phases of Nb_2O_5 can be formed under different annealing temperatures.[49] However to avoid the formation of large clusters of MWCNTs and glucose derived carbons (see Figure SI.2), and hence maintain a significantly accessible surface area, the annealing conditions were optimised and kept mild in this work.

Figure 1a shows XRD patterns for the Nb_2O_5/g-CNT, g-CNT (i.e. the pure glucose derived carbon/MWCNT material) and pristine Nb_2O_5. Diffraction peaks at 22.7°, 28.6°, 36.7°, 46.2° and 55.2° in the pattern for pristine Nb_2O_5 can be indexed as the (100), (210), (310), (410) and (610) reflections for pseudohexagonal Nb_2O_5 (TT-Nb_2O_5, PDF #07-0061); the same peaks can be found in the XRD pattern of the Nb_2O_5/g-CNT composite. The TT-Nb_2O_5 has similar XRD pattern to the orthorhombic Nb_2O_5 (T-Nb_2O_5) but with lower crystallinity.[50,51] It has been proposed that the TT-Nb_2O_5 is consists of a disordered sub-cell domain in an orthorhombic superlattice (Figure 1b), which provides more sites for defects in the unit cell.[50,51] The intensity enhancement of the broad peak observed at $2\theta \approx 26°$ in the Nb_2O_5/g-CNT can be attributed to typical (002) plane from the g-CNT.[52] Together these data indicate the successful synthesis of a Nb_2O_5/g-CNT

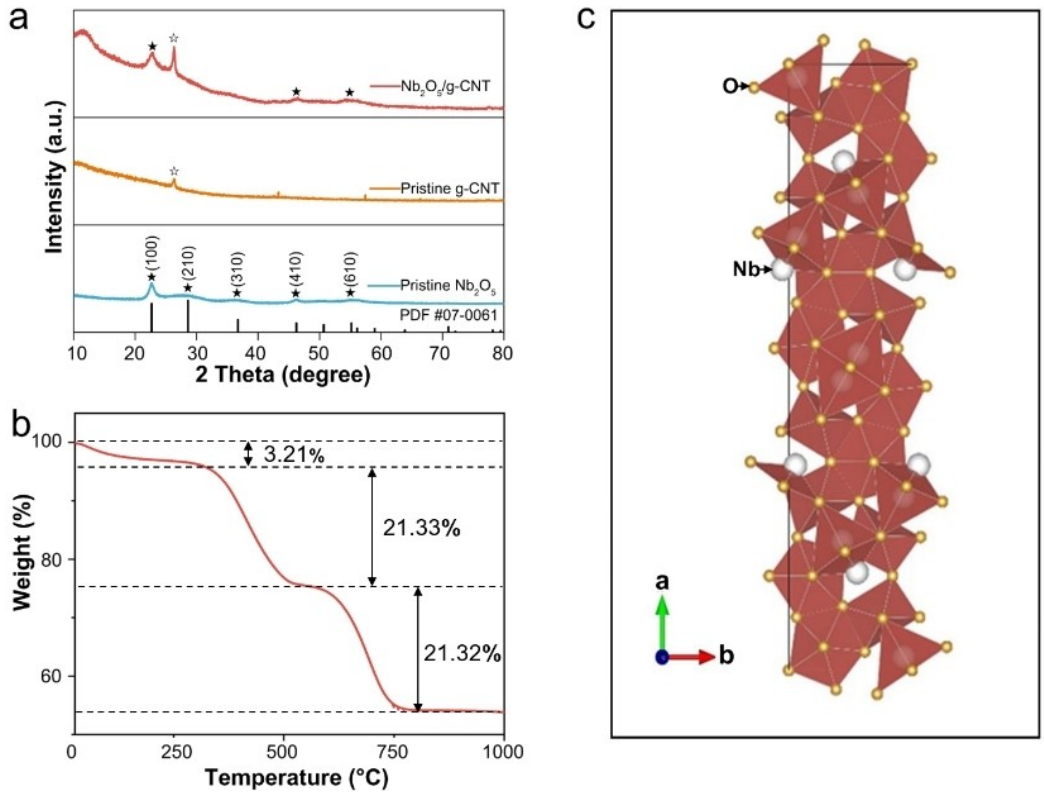

Figure 1. (a) XRD patterns of the Nb_2O_5/gCNT composite and pristine components; (b)TGA curve of the Nb_2O_5/gCNT composite and (c) the crystal structure of TT-Nb_2O_5.

composite. The average size of the TT-Nb_2O_5 crystals can be estimated to be ~8.5 nm via the Debye-Scherrer equation:

$$d = \frac{0.9\lambda}{\beta \cos\theta} \quad (1)$$

where λ is the wavelength of the X-ray, β is the full width at half maximum (FWHM) of the diffraction peak and θ is the diffraction angle.

Consistent with the study of Liu et al.,[53] in the XRD pattern of the pristine Nb_2O_5 the (001) reflection has the highest intensity, different from the standard XRD pattern of T-Nb_2O_5. This may indicate that the growth of the Nb_2O_5 nanoparticles is growth-oriented to follow the [001] direction, which produces a needle-like shape[54] in the Nb_2O_5 (see below).

The bulk composition of the Nb_2O_5/g-CNT was analysed by thermogravimetric analysis (TGA, Figure 1c) in air. While the mass loss of 3.21% from room temperature to 233 °C can be attributed to the removal of adsorbed water, losses from 262 °C to 546 °C, constituting 21.33% of the sample, can be attributed to the loss of amorphous carbon.[55] The further loss of 21.32% between 571 °C and 787 °C can be assigned to the combustion of more ordered MWCNTs in the sample.[56–58] The ~54% mass remaining above 787 °C represents the more thermally stable Nb_2O_5. Hence the Nb_2O_5:C ratio is close to 1.3:1.

X-ray photoelectron spectroscopy (XPS) further confirms the surface chemical state of the composite, with the survey spectrum of Nb_2O_5/g-CNT (Figure 2a) showing only peaks for C, O and Nb, indicating no contamination from synthetic by-products (e.g. N). The peaks of the C1s spectrum (Figure 2b) located at 284.9 eV, 286.0 eV, 287.3 eV, 289.2 eV and 291.1 eV correspond to C–C, C–O, C=O, O–C=O, and π*π transition losses, respectively.[59–61] The existence of these chemical states illustrates the existence of heteroatom-containing functional groups on the surface of the Nb_2O_5/g-CNT composite. The peak in the O 1s spectrum (Figure 2c) centred at 530.5 eV can be assigned to the Nb–O bond, whereas the one centred at 532.2 eV corresponds to the organic C=O bond and the peak centred at 533.6 eV represents the C–O bond.[62] Figure 2d presents the XPS spectrum of Nb 3d. The peaks located at 207.4 eV and 210.2 eV derive from the Nb^{5+} $3d_{5/2}$ and Nb^{5+} $3d_{3/2}$, respectively.[32] Additionally, the XPS fitting spectra of pristine MWCNTs and pristine Nb_2O_5 are shown in Figure SI 2. Pristine MWCNTs (Figure SI 2.a) exhibit a dominating carbon peak at 284.9 eV, with additional peaks at 285.0 eV, 286.3 eV and 290.3 eV related to C–O, C=O and π*π transition loss, respectively.[60,63] The peaks at 534.1 eV and 532.7 eV in O1s spectrum of pristine MWCNTs (Figure SI 2.b) are attributed to the C–O and C=O bonds,[64] whereas the peaks centred at 531.0 eV in the O1s spectrum of pristine Nb_2O_5 (Figure SI 2.d) consistent with lattice oxygen in Nb_2O_5.[65,66] In the XPS spectrum of the pure MWCNTs no significant O–C=O signature is detected, whereas a notable contribution can be observed for

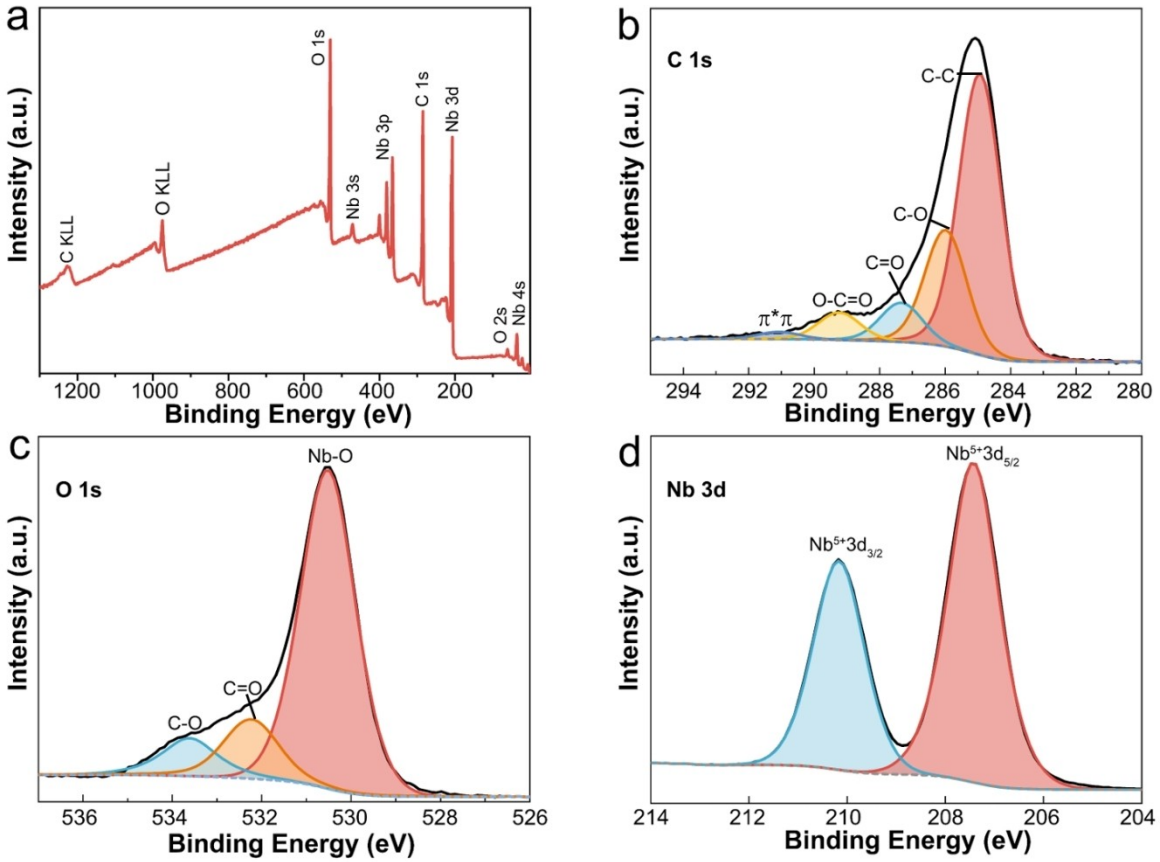

Figure 2. (a) XPS survey spectrum of the Nb_2O_5/gCNT and fitted (b) C1s; (c) O1s and (d) Nb 3d spectra.

the Nb_2O_5/g-CNT, confirming the presence of the glucose derived carbon that links the MWCNTs and Nb_2O_5.

The morphology of the Nb_2O_5/g-CNT composite material was assessed by scanning electron microscopy (SEM, Figure 3a–b). The MWCNTs could be observed to be uniformly covered along their length by a thin coating of Nb_2O_5 nano-particles, maximising the electrical contact and surface area. The N_2 adsorption-desorption measurement was performed to investigate the Brunauer-Emmett-Teller (BET) surface area and the pore structure of the Nb_2O_5/g-CNT composite (as shown in Figure SI 4). The BET results confirm the average pore diameter of 57.9 Å and the pore sizes are distributed evenly around a diameter of 50 Å. The type IV isothermal model of the BET further confirms that the composite belongs to the family of mesoporous materials. The BET surface area of the materials is 504.19 $m^2 g^{-1}$, which is a very high value that can provide a large number of active sites for sodium de/intercalation during cycling.[67] The high surface contact area can also be seen in TEM images (Figure 3c–d), which reveal further structural details of the composite. In Figure 3c. both the high surface area Nb_2O_5 and a section of uncoated MWCNT coated in amorphous carbon, which was generated by the reduction of glucose during the hydrothermal reaction, can be seen. The amorphous carbon is expected to link the CNTs strongly to the Nb_2O_5 nanoparticles. It can also be seen that the Nb_2O_5 coating is composed of numerous needle-like nano-rods, resulting in a high surface area urchin-like structure (Figure 3d.). The observed morphology of the Nb_2O_5/g-CNT composite is expected to give rise to three mechanisms for the enhancement of electrochemical performance. First, the micro-nanostructure of the composite nanorods will enlarge their contact area with the electrolyte and thereby improve cell mass transport[68]. Second, the homogeneous wrapping of the Nb_2O_5 nanoparticles and CNTs will lead to enhanced electrical conductivity to the semiconducting metal oxide, ensuring high material utilisation and improvement in surface charge transfer.[69] Third, CNTs are known to be mechanically strong and flexible, meaning they will enhance the ability of the electrode to endure mechanical stresses, e.g. by volume expansion.[70]

The cycling performance of Nb_2O_5/g-CNT in SIBs was evaluated through galvanostatic charge-discharge (GCD). The initial three GCD cycles at a current density of 0.2 $A g^{-1}$ are presented in Figure 4a. While the initial high discharge capacity of 510 $mAh g^{-1}$ is indicative of irreversible capacity losses due to solid electrolyte interface (SEI) formation on the high surface area MWCNT and glucose-derived carbon, it quickly establishes a reversible capacity of 203 $mAh g^{-1}$ on cycle two (Figure 4c, showing cycle 2–300). The specific capacity stabilises at ~135 $mAh g^{-1}$ after ~25 cycles at 0.2 $A g^{-1}$ where it remains until cycle 300, with a Coulombic efficiency (CE) of ~99.6%. The contribution of g-CNT to the capacity has also been studied (see Figure SI 7) and while the initial capacity was high (~

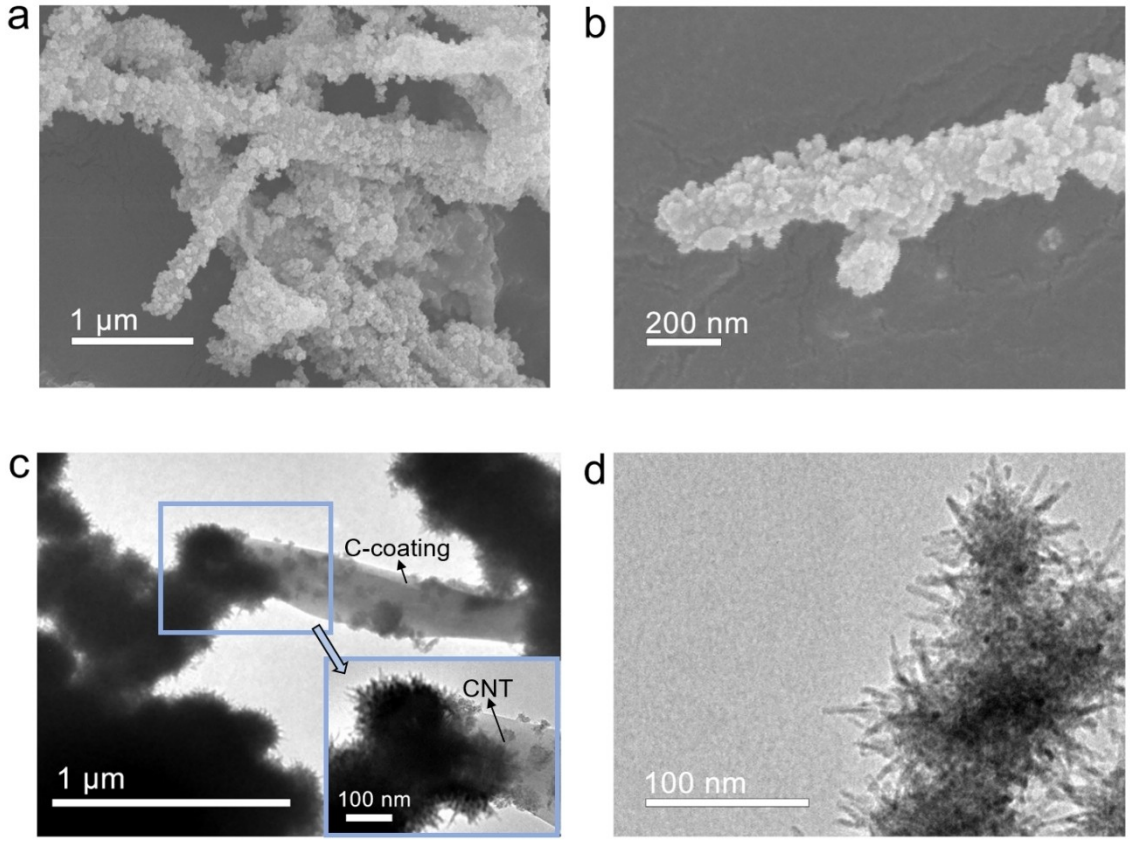

Figure 3. (a–b) SEM and (c–d) TEM images of the Nb_2O_5/g-CNT composite.

304 mAh g^{-1}), likely due to parasitic processes, this decayed quickly to ~67 mAh g^{-1} after 20 cycles.

Figure 4b shows the rate performance of the Nb_2O_5/g-CNT composite, pristine Nb_2O_5 and a simple mix of pristine Nb_2O_5 and g-CNTs (Nb_2O_5 + g-CNT mixture, i.e. no co-synthesis) at different current densities. The Nb_2O_5/g-CNT composite produced via the hydrothermal co-synthesis delivers a significantly superior specific capacity at all current densities, when compared to the pristine Nb_2O_5 and Nb_2O_5 + gCNT mixture. This provides strong evidence that simple combination of Nb_2O_5 and carbonaceous materials is not sufficient to overcome the issues of low conductivity. The measured specific capacities of the Nb_2O_5/g-CNT at 0.1, 0.2, 0.5 1, 2 and 5 A g^{-1} were 167, 148, 127, 107, 86 and 53 mAh g^{-1}, demonstrating good capacity retention at high rates. Moreover, 97% of the specific capacity (~ 163 mAh g^{-1}) can be recovered after cycling at high rates, showing the composite material offers outstanding invertibility when compared to other Nb_2O_5-based SIB anodes reported in the literature.[35,71–73]

To study the kinetics and energy storage mechanisms of the Nb_2O_5/g-CNT as anodes for SIBs, cyclic voltammetry (CV) profiles were collected. The curves of the first three CV cycles at 0.1 mV s^{-1} are presented in Figure 5a. The distinct difference between the first CV cycle and the 2nd cycle further highlights the formation of the SEI film below 1.5 V (vs. Na/Na$^+$), which causes irreversible capacity losses. However, importantly these losses are confined to the first cycle, indicating the SEI formed is strong and stable. The CV curves at different scan rates (Figure 5b) exhibit similar shapes as common pseudocapacitive metal oxide materials.[74] The broad reduction peak and oxidation peak at around 0.5 V correspond to the sodiation and de-sodiation processes. The kinetic process of sodium storage can be studied by analysing the relationship between current (i) and scan rate (v):[44,75]

$$i = av^b \tag{2}$$

$$\log i = b\log v + \log a \tag{3}$$

The b-value reflects the kinetic behaviour of the material: when the b-value equals 0.5, the process is diffusion behaviour dominated; when the b-value equals 1, the process is controlled by capacitive behaviour.[76] Linear fits of the anodic and cathodic peak currents are shown in Figure 5c. The b-value of the anodic and cathodic reactions, which can be found from the slope of the linear fits of the anodic and cathodic peaks, are 0.89 and 0.94, respectively. The electrochemical reaction of the Nb_2O_5/g-CNT electrode is therefore dominated by pseudocapacitive behaviour.[77,78] To further determine the contribution of kinetically fast pseudocapacitive reactions quantitatively, the capacitive ratios were calculated using the equation:[79,80]

$$i(v) = k_1 v + k_2 v^{0.5} \tag{4}$$

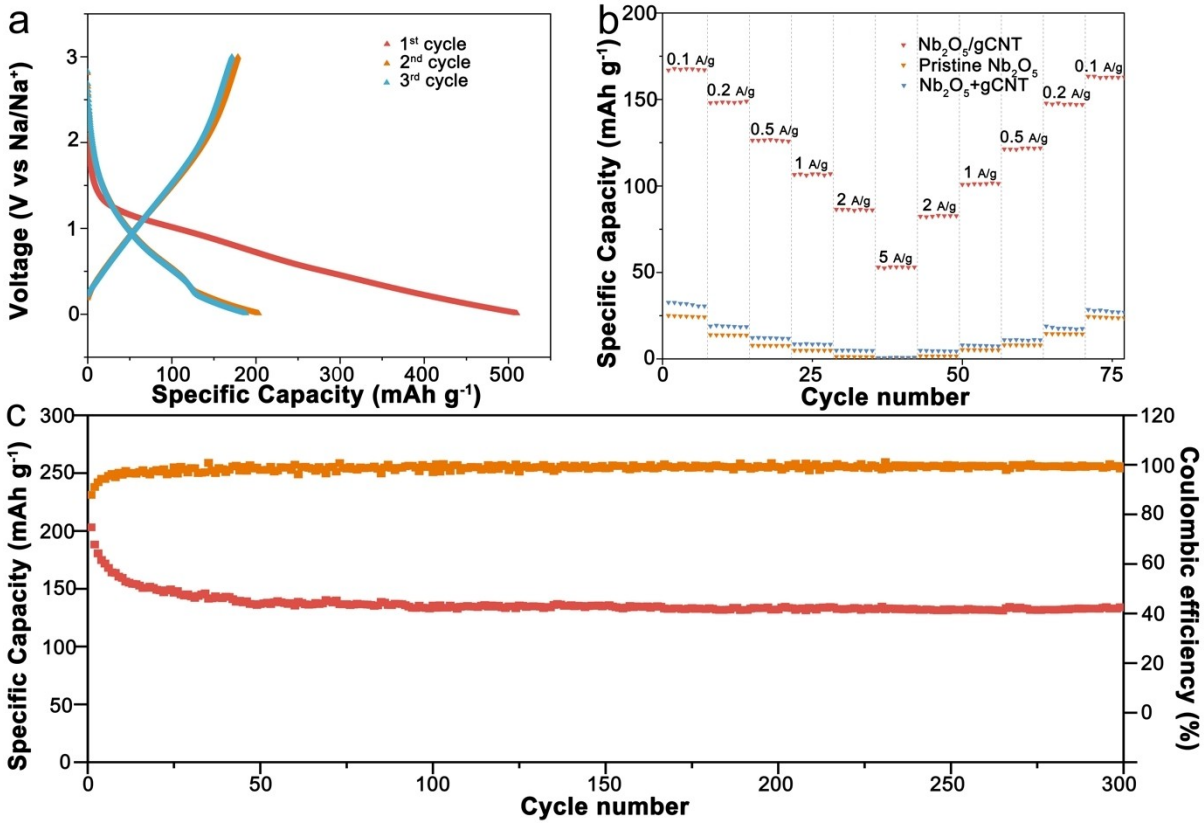

Figure 4. (a) Charge/discharge profile of the Nb_2O_5/g-CNT (1.09 mg/cm^2) SIB at 0.2 A g^{-1}; (b) Rate capability of the Nb_2O_5/g-CNT (1.18 mg/cm^2), pristine Nb_2O_5 and Nb_2O_5 + CNT mixture in SIBs; (c) Long cycling performance of Nb_2O_5/g-CNT (1.09 mg/cm^2) at 0.2 A g^{-1} in SIBs.

where i is the current, v is the scan rate and k_1, k_2 are variables. In Eq (4), (k_1v) is the capacitive element and ($k_2v^{0.5}$) is the diffusion-limited element and hence the capacitive ratio at different scan rates can be calculated (Figure SI 8). Figure 5d shows the contribution ratio of capacitive and diffusion behaviour of Nb_2O_5/g-CNT at various scan rates, showing ~83% of the total capacity contribution of the Nb_2O_5/g-CNT derived from pseudocapacitive processes at 0.5 mV s^{-1}, which highlights its extremely fast kinetics and explains its excellent rate capability. This electrochemical behaviour is expected to be due to the nano-scale particle size of Nb_2O_5, combined with the highly conductive network and high surface area provided by the CNTs, provides both short ion diffusion pathways and efficient electron transfer at the electrode/electrolyte interface.

Conclusion

In summary, here a pseudohexagonal Nb_2O_5/g-CNT composite consisting of urchin-like TT-Nb_2O_5 nanoparticles strongly bonded to a highly conductive MWCNT support through a glucose-derived carbon, was successfully synthesised via a hydrothermal-annealing processes and assessed as an anode for SIBs. The composite, which represents the first analysis of low-cost TT-Nb_2O_5 in SIBs, was shown to offer a high specific capacity (203 mAh g^{-1} at 0.2 A g^{-1}) and importantly it was able to retain a significant capacity at high rates (up to 5 A g^{-1}) and after significant cycle lifetimes (~135 mAh g^{-1} after 300 cycles). This enhanced behaviour is attributed to the superior electrical conductivity and connectivity, optimal mass transport conditions and the mechanical strength and durability established by the strongly linked Nb_2O_5 and MWCNT network. This methodology therefore represents a promising and simple to implement at scale route for the application of high-capacity metal oxides in highly reversible SIBs.

Author Contributions

Guanxu Chen was responsible for the design of the project, experiments including synthesis, material characterisation, electrochemical characterisation and writing of the manuscript. Jintao Chen conducted the XPS. Ivan P. Parkin provided equipment for material synthesis. Thomas S. Miller and Guanjie He designed and supervised the project. All authors contributed to the review of manuscript.

Acknowledgements

T.S.M. thanks the Faraday Institution (EP/S003053/1) for support via the LiSTAR project (FIRG014).

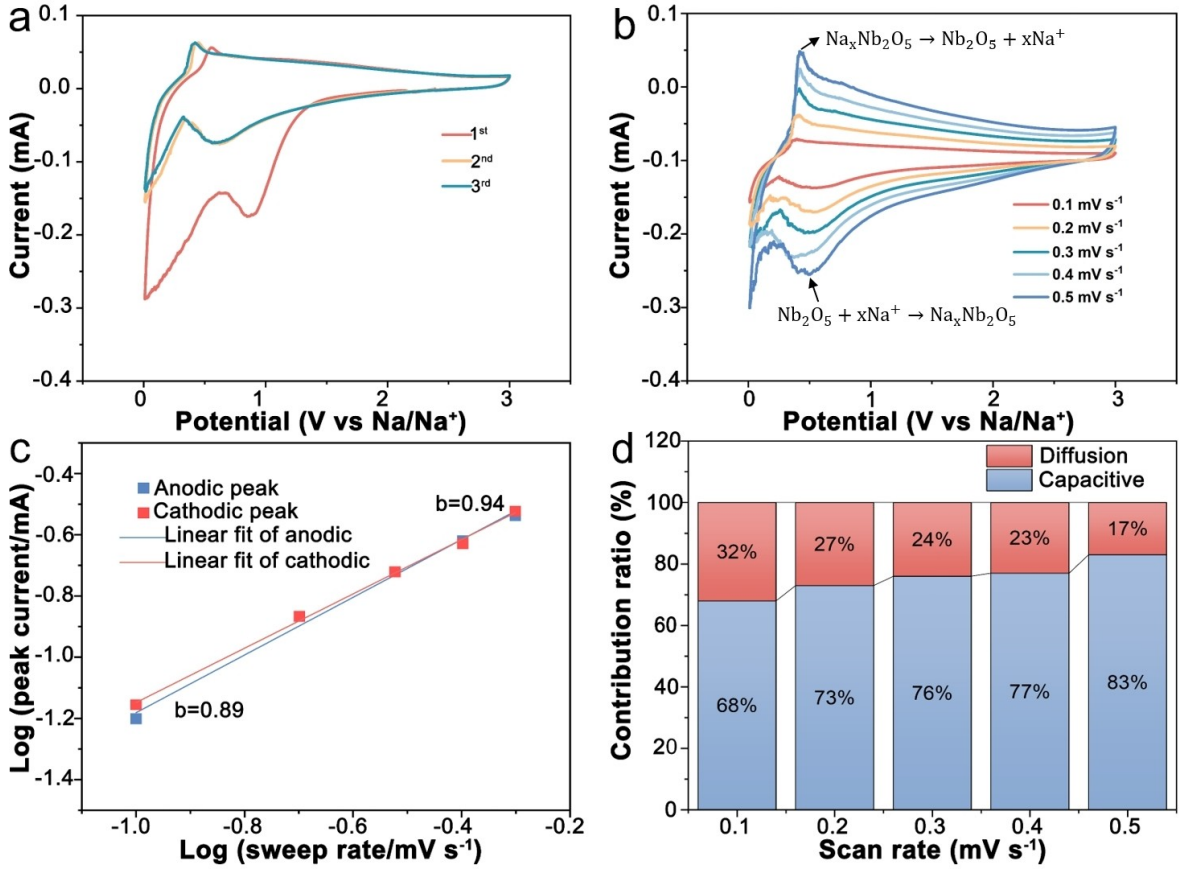

Figure 5. (a) CV curves of the Nb_2O_5/g-CNT for the initial three cycles at 0.1 mV s^{-1}; (b) CV curves of the Nb_2O_5/g-CNT at different scan rates; (c) the logarithmic relationship between the peak currents and scan rates; (d) contribution ratio of capacitive and diffusion process to the capacity of the Nb_2O_5/g-CNT at different scan rates.

Conflict of Interest

The authors declare no conflict of interest.

Data Availability Statement

The data that support the findings of this study are available from the corresponding author upon reasonable request.

Keywords: Battery anode · Carbon nanomaterials · NIB · Niobium oxide · SIB

[1] W. Zhang, Y. Liu, Z. Guo, *Sci. Adv.* **2019**, *5*, 7412–7422.
[2] M. Sha, L. Liu, H. Zhao, Y. Lei, *Carbon Energy* **2020**, *2*, 350–369.
[3] T. Perveen, M. Siddiq, N. Shahzad, R. Ihsan, A. Ahmad, M. I. Shahzad, *Renewable Sustainable Energy Rev.* **2020**, *119*, 109549.
[4] R. Ding, Y. Huang, G. Li, Q. Liao, T. Wei, Y. Liu, Y. Huang, H. He, *Front. Chem.* **2020**, *8*, 1175.
[5] X. Chen, Y. Fang, J. Tian, H. Lu, X. Ai, H. Yang, Y. Cao, *ACS Appl. Mater. Interfaces* **2021**, *13*, 18914–18922.
[6] L. Xiao, H. Lu, Y. Fang, M. L. Sushko, Y. Cao, X. Ai, H. Yang, J. Liu, *Adv. Energy Mater.* **2018**, *8*, 1703238.
[7] X. F. Luo, C. H. Yang, Y. Y. Peng, N. W. Pu, M. der Ger, C. te Hsieh, J. K. Chang, *J. Mater. Chem. A* **2015**, *3*, 10320–10326.
[8] L. Yue, L. Yue, H. Zhao, Z. Wu, J. Liang, S. Lu, G. Chen, S. Gao, B. Zhong, X. Guo, X. Sun, *J. Mater. Chem. A* **2020**, *8*, 11493–11510.
[9] J. Xu, M. Wang, N. P. Wickramaratne, M. Jaroniec, S. Dou, L. Dai, J. Xu, M. Wang, L. Dai, S. Dou, N. P. Wickramaratne, M. Jaroniec, *Adv. Mater.* **2015**, *27*, 2042–2048.
[10] J. Zhu, C. Chen, Y. Lu, Y. Ge, H. Jiang, K. Fu, X. Zhang, *Carbon N Y* **2015**, *94*, 189–195.
[11] W. Luo, J. Schardt, C. Bommier, B. Wang, J. Razink, J. Simonsen, X. Ji, *J. Mater. Chem. A* **2013**, *1*, 10662–10666.
[12] Y. Cao, Q. Ye, F. Wang, X. Fan, L. Hu, F. Wang, T. Zhai, H. Li, Y. Cao, Q. Ye, F. F. Wang, X. L. Fan, L. T. Hu, F. K. Wang, T. Y. Zhai, H. Q. Li, *Adv. Funct. Mater.* **2020**, *30*, 2003733.
[13] K. Li, H. Liu, G. Wang, K. Li, H. Liu, G. Wang, *Arabian J. Sci. Eng.* **2014**, *39*, 6589–6593.
[14] I. Sultana, M. M. Rahman, S. Mateti, V. G. Ahmadabadi, A. M. Glushenkov, Y. Chen, *Nanoscale* **2017**, *9*, 3646–3654.
[15] W. Zhong, M. Tao, W. Tang, W. Gao, T. Yang, Y. Zhang, R. Zhan, S.-J. Bao, M. Xu, *Chem. Eng. J.* **2019**, *378*, 122209.
[16] S. Fu, J. Ni, Y. Xu, Q. Zhang, L. Li, *Nano Lett.* **2016**, *16*, 4544–4551.
[17] W. Luo, F. Shen, C. Bommier, H. Zhu, X. Ji, L. Hu, *Acc. Chem. Res.* **2016**, *49*, 231–240.
[18] Y. Liang, W.-H. Lai, Z. Miao, S.-L. Chou, *Small* **2018**, *14*, 1702514.
[19] S. Fang, D. Bresser, S. Passerini, *Adv. Energy Mater.* **2020**, *10*, 1902485.
[20] E. Goikolea, V. Palomares, S. Wang, I. R. de Larramendi, X. Guo, G. Wang, T. Rojo, *Adv. Energy Mater.* **2020**, *10*, 2002055.
[21] C. H. Lau, R. Cervini, S. R. Clarke, M. G. Markovic, J. G. Matisons, S. C. Hawkins, C. P. Huynh, G. P. Simon, *J. Nanopart. Res.* **2008**, *10*, 77–88.
[22] D. Goonetilleke, J. C. Pramudita, M. Choucair, A. Rawal, N. Sharma, *J. Power Sources* **2016**, *314*, 102–108.
[23] A. P. Vijaya Kumar Saroja, M. Muruganathan, K. Muthusamy, H. Mizuta, R. Sundara, *Nano Lett.* **2018**, *18*, 5688–5696.

[24] K. A. Wepasnick, B. A. Smith, K. E. Schrote, H. K. Wilson, S. R. Diegelmann, D. H. Fairbrother, *Carbon N Y* **2011**, *49*, 24–36.
[25] Y. Liang, W.-H. Lai, Z. Miao, S.-L. Chou, *Small* **2018**, *14*, 1702514.
[26] X. Wang, G. Li, Z. Chen, V. Augustyn, X. Ma, G. Wang, B. Dunn, Y. Lu, *Adv. Energy Mater.* **2011**, *1*, 1089–1093.
[27] Z. Chen, W. Chen, H. Wang, Z. Xiao, F. Yu, *Nanoscale* **2020**, *12*, 18673–18681.
[28] H. Park, D. Lee, T. Song, *J. Power Sources* **2019**, *414*, 377–382.
[29] M. Wei, K. Wei, M. Ichihara, H. Zhou, *Electrochem. Commun.* **2008**, *7*, 980–983.
[30] Y. Liu, L. Lin, W. Zhang, M. Wei, *Sci. Rep.* **2017**, *7*, 1–9.
[31] M. Lübke, A. Sumboja, I. D. Johnson, D. J. L. Brett, P. R. Shearing, Z. Liu, J. A. Darr, *Electrochim. Acta* **2016**, *192*, 363–369.
[32] X. Zhang, J. Wang, X. Wang, Y. Li, Y. Zhao, Z. Bakenov, G. Li, *Appl. Surf. Sci.* **2021**, *567*, 150862.
[33] Z. Bi, Y. Zhang, X. Li, Y. Liang, W. Ma, Z. Zhou, M. Zhu, *Electrochim. Acta* **2022**, *411*, 140070.
[34] L. Yan, G. Chen, S. Sarker, S. Richins, H. Wang, W. Xu, X. Rui, H. Luo, *ACS Appl. Mater. Interfaces* **2016**, *8*, 22213–22219.
[35] L. Yang, Y.-E. Zhu, J. Sheng, F. Li, B. Tang, Y. Zhang, Z. Zhou, L. P. Yang, Y. Zhu, J. Sheng, F. Li, B. Tang, Y. Zhang, Z. Zhou, *Small* **2017**, *13*, 1702588.
[36] H. Ding, Z. Song, H. Zhang, H. Zhang, X. Li, *Mater Today Nano* **2020**, *11*, 100082.
[37] L. Wang, X. Bi, S. Yang, L. Wang, X. Bi, S. Yang, *Adv. Mater.* **2016**, *28*, 7672–7679.
[38] X. Wang, Q. Li, L. Zhang, Z. Hu, L. Yu, T. Jiang, C. Lu, C. Yan, J. Sun, Z. X. Liu, G Wang, Q. C. Li, L. Zhang, Z. L. Hu, L. H. Yu, T. Jiang, C. Lu, C. Yan, J. Y. Sun, Z. F. Liu, *Adv. Mater.* **2018**, *30*, 1800963.
[39] L. Kong, X. Cao, J. Wang, W. Qiao, L. Ling, D. Long, *J. Power Sources* **2016**, *309*, 42–49.
[40] Y. Lian, Y. Zheng, Y. Bai, D. Wang, H. Yan, Z. Wang, J. Zhao, H. Zhang, *J. Power Sources* **2021**, *507*, 230267.
[41] X. Wen, K. Xiang, Y. Zhu, L. Xiao, H. Liao, X. Chen, H. Chen, *Ind Eng Chem Res* **2019**, 58, 8724–8733.
[42] C. Shi, K. Xiang, Y. Zhu, X. Chen, W. Zhou, H. Chen, *Electrochim. Acta* **2017**, *246*, 1088–1096.
[43] S. Li, T. Wang, W. Zhu, J. Lian, Y. Huang, Y.-Y. Yu, J. Qiu, Y. Zhao, Y.-C. Yong, H. Li, *J. Mater. Chem. A* **2019**, *7*, 693–703.
[44] N. Li, F. Zhang, Y. Tang, *J. Mater. Chem. A* **2018**, *6*, 17889–17895.
[45] Z. Chen, W. Chen, H. Wang, Z. Xiao, F. Yu, *Nanoscale* **2020**, *12*, 18673–18681.
[46] Y. Zhang, L. Fang, *IOP Conf Ser Earth Environ Sci* **2020**, *619*, 012015.
[47] Z. Tong, R. Yang, S. Wu, D. Shen, T. Jiao, K. Zhang, W. Zhang, C.-S. Lee, Z. Tong, R. Yang, D. Shen, C. Lee, S. Wu, T. Jiao, W. Zhang, K. Zhang, *Small* **2019**, *15*, 1901272.
[48] Y. X. Gan, A. H. Jayatissa, Z. Yu, X. Chen, M. Li, *J. Nanomater.* **2020**, *2020*, DOI 10.1155/2020/8917013.
[49] L. Yan, X. Rui, G. Chen, W. Xu, G. Zou, H. Luo, *Nanoscale* **2016**, *8*, 8443–8465.
[50] G. Falk, M. Borlaf, M. J. López-Muñoz, J. C. Fariñas, J. B. Rodrigues Neto, R. Moreno, *J. Mater. Res.* **2017**, *32*, 3271–3278.
[51] C. Valencia-Balvín, S. Pérez-Walton, G. M. Dalpian, J. M. Osorio-Guillén, *Comput. Mater. Sci.* **2014**, *C*, 133–140.
[52] A. Cao, C. Xu, J. Liang, D. Wu, B. Wei, *Chem. Phys. Lett.* **2001**, *344*, 13–17.
[53] X. Liu, G. Liu, Y. Liu, R. Sun, J. Ma, J. Guo, M. Hu, *Dalton Trans.* **2017**, *46*, 10935–10940.
[54] Y. Wang, F. Xin, X. Yin, Y. Song, T. Xiang, J. Wang, *J. Phys. Chem. C* **2018**, *122*, 2155–2164.
[55] T. Suzuki, S. Inoue, Y. Ando, *J. Nanosci. Nanotechnol.* **2010**, *10*, 3924–3928.
[56] D. Bom, R. Andrews, D. Jacques, J. Anthony, B. Chen, M. S. Meier, J. P. Selegue, *Nano Lett.* **2002**, *2*, 615–619.
[57] A. M. Baker, L. Wang, S. G. Advani, A. K. Prasad, *J. Mater. Chem.* **2012**, *22*, 14008–14012.
[58] R. Yudianti, L. Indrarti, H. Onggo, *J. Appl. Sci.* **2010**, *10*, 1978–1982.
[59] C. Shi, K. Xiang, Y. Zhu, X. Chen, W. Zhou, H. Chen, *Electrochim. Acta* **2017**, *246*, 1088–1096.
[60] V. Datsyuk, M. Kalyva, K. Papagelis, J. Parthenios, D. Tasis, A. Siokou, I. Kallitsis, C. Galiotis, *Carbon N Y* **2008**, *46*, 833–840.
[61] S. Kundu, Y. Wang, W. Xia, M. Muhler, *J. Phys. Chem. C* **2008**, *112*, 16869–16878.
[62] K. Islam, R. Sultana, A. Rakshit, U. K. Goutam, S. Chakraborty, *SN Appl Sci* **2020**, *2*, 1–7.
[63] H. J. Lee, W. S. Choi, T. Nguyen, Y. B. Lee, H. Lee, *Carbon N Y* **2011**, *49*, 5150–5157.
[64] D. Kolacyak, J. Ihde, C. Merten, A. Hartwig, U. Lommatzsch, *J. Colloid Interface Sci.* **2011**, *359*, 311–317.
[65] P. Nagaraju, R. Vasudevan, A. Alsalme, A. Alghamdi, M. Arivanandhan, R. Jayavel, *Nanomaterials* **2020**, *10*, 160.
[66] Ö. D. Coşkun, S. Demirel, G. Atak, *J. Alloys Compd.* **2015**, *648*, 994–1004.
[67] S. Li, J. Qiu, C. Lai, M. Ling, H. Zhao, S. Zhang, *Nano Energy* **2015**, *12*, 224–230.
[68] T. Yang, Z. Yang, X. Cheng, Y. Ding, Y. Fan, G. Liu, K. Zhang, S. Jin, X. Liu, Z. Qiao, *J. Alloys Compd.* **2021**, *876*, 160145.
[69] E. Lim, C. Jo, M. S. Kim, M.-H. Kim, J. Chun, H. Kim, J. Park, K. C. Roh, K. Kang, S. Yoon, J. Lee, *Adv. Funct. Mater.* **2016**, *26*, 3711–3719.
[70] F. Tao, Y. Liu, X. Ren, A. Jiang, H. Wei, X. Zhai, F. Wang, H. R. Stock, S. Wen, F. Ren, *J. Alloys Compd.* **2021**, *873*, 159742.
[71] Z. Chen, W. Chen, H. Wang, Z. Xiao, F. Yu, *Nanoscale* **2020**, *12*, 18673–18681.
[72] X. Zhang, J. Wang, X. Wang, Y. Li, Y. Zhao, Z. Bakenov, G. Li, *Appl. Surf. Sci.* **2021**, *567*, 150862.
[73] Y. Zhang, L. Fang, *IOP Conf Ser Earth Environ Sci* **2020**, *619*, 012015.
[74] Y. Jiang, J. Liu, *Energy Environ. Mater.* **2019**, *2*, 30–37.
[75] H. Li, Y. Zhu, S. Dong, L. Shen, Z. Chen, X. Zhang, G. Yu, *Chem. Mater.* **2016**, *28*, 5753–5760.
[76] P. Yu, C. Li, X. Guo, *J. Phys. Chem. C* **2014**, *118*, 10616–10624.
[77] T. P. Mofokeng, A. Kabir Ipadeola, Z. Nobuntu Tetana, K. I. Ozoemena, *ACS Omega* **2020**, *5*, DOI 10.1021/acsomega.0c02563.
[78] B. Shang, Q. Peng, X. Jiao, G. Xi, X. Hu, *Ionics (Kiel)* **2019**, *25*, 1679–1688.
[79] S. Fu, Q. Yu, Z. Liu, P. Hu, Q. Chen, S. Feng, L. Mai, L. Zhou, *J. Mater. Chem. A* **2019**, *7*, 11234–11240.
[80] J. Yuan, X. Li, J. Liu, S. Zuo, X. Li, F. Li, Y. Gan, H. He, X. Xu, X. Zhang, J. Meng, *J. Colloid Interface Sci.* **2022**, *613*, 84–93.

Manuscript received: July 26, 2022
Revised manuscript received: September 18, 2022
Accepted manuscript online: September 19, 2022

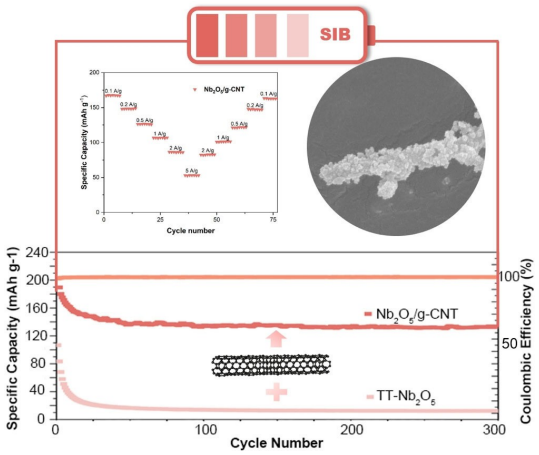

G. Chen, J. Chen, Prof. I. P. Parkin, Dr. G. He, Dr. T. S. Miller**

1 – 9

Pseudohexagonal Nb_2O_5-Decorated Carbon Nanotubes as a High-Performance Composite Anode for Sodium Ion Batteries

Pseudohexagonal Nb_2O_5 (TT-Nb_2O_5) has been applied in sodium ion batteries (SIBs) for the first time. Lower synthesis temperatures, improved conductivity and stability were achieved by the introduction of a designed carbon framework. The TT-Nb_2O_5/carbon nanotube composite exhibits high specific capacity (135 mAh g^{-1} at 0.2 A g^{-1}) in long cycles and good rate capability (53 mAh g^{-1} at high current density of 5 A g^{-1}). The outstanding electrochemical performance is attributed to the superior electrical conductivity and connectivity, optimal mass transport conditions and the mechanical strength and durability established by the strongly linked TT-Nb_2O_5 and MWCNT network. This study provides a cost-effective route to the application of Nb_2O_5 in SIBs.